Analysis of the breakdown spot spatial distribution in Pt/HfO_2/Pt capacitors using nearest neighbor statistics

X. Saura, J. Suñé, S. Monaghan, P. K. Hurley, and E. Miranda

Citation: Journal of Applied Physics **114**, 154112 (2013); doi: 10.1063/1.4825321
View online: http://dx.doi.org/10.1063/1.4825321
View Table of Contents: http://aip.scitation.org/toc/jap/114/15
Published by the American Institute of Physics

JOURNAL OF APPLIED PHYSICS **114**, 154112 (2013)

Analysis of the breakdown spot spatial distribution in Pt/HfO_2/Pt capacitors using nearest neighbor statistics

X. Saura,[1] J. Suñé,[1] S. Monaghan,[2] P. K. Hurley,[2] and E. Miranda[1]
[1]*Departament d'Enginyeria Electrònica, Universitat Autònoma de Barcelona, 08193 Cerdanyola del Valles, Barcelona, Spain*
[2]*Tyndall National Institute, University College Cork, Cork, Ireland*

(Received 20 August 2013; accepted 1 October 2013; published online 21 October 2013)

The breakdown spot spatial distribution in Pt/HfO_2/Pt capacitors is investigated using nearest neighbor statistics in combination with more conventional estimation methods such as the point-event and event-event distance distributions. The spots appear as a random point pattern over the top metal electrode and arise as a consequence of significant localized thermal effects caused by the application of high-voltage ramped stress to the devices. The reported study mainly involves the statistical characterization of the distances between each failure site and the nearest, second nearest, … *k*th nearest event and the comparison with the corresponding theoretical distributions for a complete spatial randomness (CSR) process. A method for detecting and correcting deviations from CSR based on a precise estimation of the average point intensity and the effective damaged device area is proposed. © *2013 AIP Publishing LLC*. [http://dx.doi.org/10.1063/1.4825321]

I. INTRODUCTION

Reliability analysis of metal-insulator-metal (MIM) and metal-insulator-semiconductor (MIS) devices typically involves electrical characterization techniques such as time-dependent dielectric breakdown (TDDB) and time-zero dielectric breakdown (TZDB) tests.[1] TDDB and TZDB tests consist in the application of constant and ramped electrical stress, respectively, until the detection of a sudden jump or an anomalous noise increment in the measured signal. These changes reveal the occurrence of a single or multiple breakdown (BD) events which physically correspond to the formation of filamentary-like leakage current paths across the dielectric film.[2] In the case of hard BD, this process is associated with important thermal effects and lateral propagation of the damage which can result in the evaporation of the metal electrode at the failure site.[3] Filamentary conduction has been previously reported to occur in SiO_2 in MIS structures[4,5] as well as in many other dielectric stacks in MIM structures mainly in connection with the resistive switching effect.[6,7] It is often assumed in reliability studies that the BD spot generation in MIM and MIS structures is well described by a 2-dimensional complete spatial randomness (CSR) process, also referred to in literature as a Poisson process.[8] This is well supported by the area dependence of the Weibull distribution for the time-to-first BD event in TDDB tests.[9] Although this spatio-temporal failure generation model is also consistent with the successive BD statistics for uncorrelated events, TDDB characterization is for practical reasons restricted to only a few breakdown events per device.[10] In general, both TDDB and TZDB do not provide direct information about the location of the failure sites over the device area unless special purpose structures are considered. In this regard, Alam *et al.*[11] were able to determine the *x* and *y* coordinates of successive BD events by tracking the evolution of the current distribution in four-terminal MIS transistors. However, because of the gate current increase after each BD event and the consequent loss of sensitivity, this Van der Pauw-like electrical localization technique is, again, limited in practice to a few events which prevents a detailed investigation of their spatial distribution. In Ref. 11, this limitation was circumvented by considering a Monte Carlo simulation of the BD spot generation process compatible with the observed current distribution at the four device terminals. On the other hand, in recent papers, we have demonstrated that it is possible to generate a large number of BD spots in MIS and MIM structures using ramped voltage stress.[12,13] As the images taken through an optical microscope reveal, the damage caused to the structures can be of such magnitude that permanent marks on the top metal plates become easily perceptible as random point patterns, which makes the application of the methods of spatial statistics feasible.[14] In addition, we demonstrated that if the number of spots is sufficiently large, it is possible to detect departures from CSR associated with a nonuniform distribution of the failure sites.[13] Although these inhomogeneities can affect first order estimators like the inter-event distance distribution as well as second order estimators like the pair correlation function, a systematic approach capable of characterizing these divergences has not been developed yet. In this work, numerical and functional estimators like the intensity plot, the event-event and the point-event distributions, which help to understand the structure of BD spot patterns in Pt/HfO_2/Pt capacitors, are discussed. An accurate method for assessing and correcting the average point intensity estimator based on a thorough analysis of the *k*th nearest neighbor distance distribution up to the fiftieth order is also reported. The statistical analysis presented in this paper was carried out using the Spatstat package for R language.[15]

II. SAMPLE FABRICATION

The statistical study of the BD spot distribution was performed on MIM capacitors with circular area electrodes of radius $R = 113$, 282, and 423 μm. The devices were fabricated as follows: 200 nm-thick thermal SiO_2 layers were

grown on n-type Si(100) substrates with resistivities of 1–4 Ω cm. MIM capacitors were formed on the insulating layers by first depositing Pt (200 nm-thick) by electron-beam (e-beam) evaporation. The samples were then placed in a Cambridge NanoTech Fiji atomic layer deposition (ALD) system where HfO_2 (30 nm-thick) was deposited using TEMAHf precursor and H_2O. The samples were then returned to the e-beam evaporator and a Pt layer (200 nm-thick) was deposited on top of the HfO_2 layer. Lithography and lift-off processes were used to form arrays of capacitors with different radius. Access to the bottom Pt metal was enabled via a dry etching technique using a mask/resist process that removes the HfO_2 to the bottom Pt metal while at the same time protecting the top Pt metal of the patterned devices. In addition, the oxide extends 25 μm beyond the perimeter edge of the top metal. The relative κ-value of the HfO_2 film extracted from capacitance-voltage measurements is 20. The probe station camera was used to capture the BD spot patterns shown in this work.

III. BD SPOT PATTERN GENERATION AND STATISTICAL ANALYSIS

Application of TZDB tests from 0 V to 8 V and from 0 V to 10 V to two capacitors with the same radius ($R = 113\ \mu$m) lead to the generation of multiple BD spots on their top metal plates as illustrated in Figs. 1(a) and 1(c), respectively. As expected, the number of spots is larger in the second case because of the higher maximum stress voltage applied. In the first case, the spot pattern consists in $N = 77$ events with an average intensity $\lambda = 1.92 \times 10^{-3}$ points/μm^2, while in the second case the pattern consists in $N = 529$ events with $\lambda = 1.32 \times 10^{-2}$ points/μm^2. λ is calculated as the number of points divided by the nominal area of the device. The degradation process is accompanied by a remarkable increase of the leakage currents that flow through the structures and which largely exceed the limit of our measurement unit (100 mA). In what follows, the BD spot patterns will be mathematically treated as point patterns, *i.e.*, the spot size will be disregarded. As it will be shown below, this has a major statistical consequence mainly in the short distance range. Figures 1(b) and 1(d) illustrate the interevent distance histograms corresponding to Figs. 1(a) and 1(c), respectively. The solid lines were calculated using the expression,

$$p(r) = \frac{2r}{R^2}\left[\frac{2}{\pi}\cos^{-1}\left(\frac{r}{2R}\right) - \frac{r}{\pi R}\sqrt{1 - \frac{r^2}{4R^2}}\right] \qquad 0 < r < 2R, \tag{1}$$

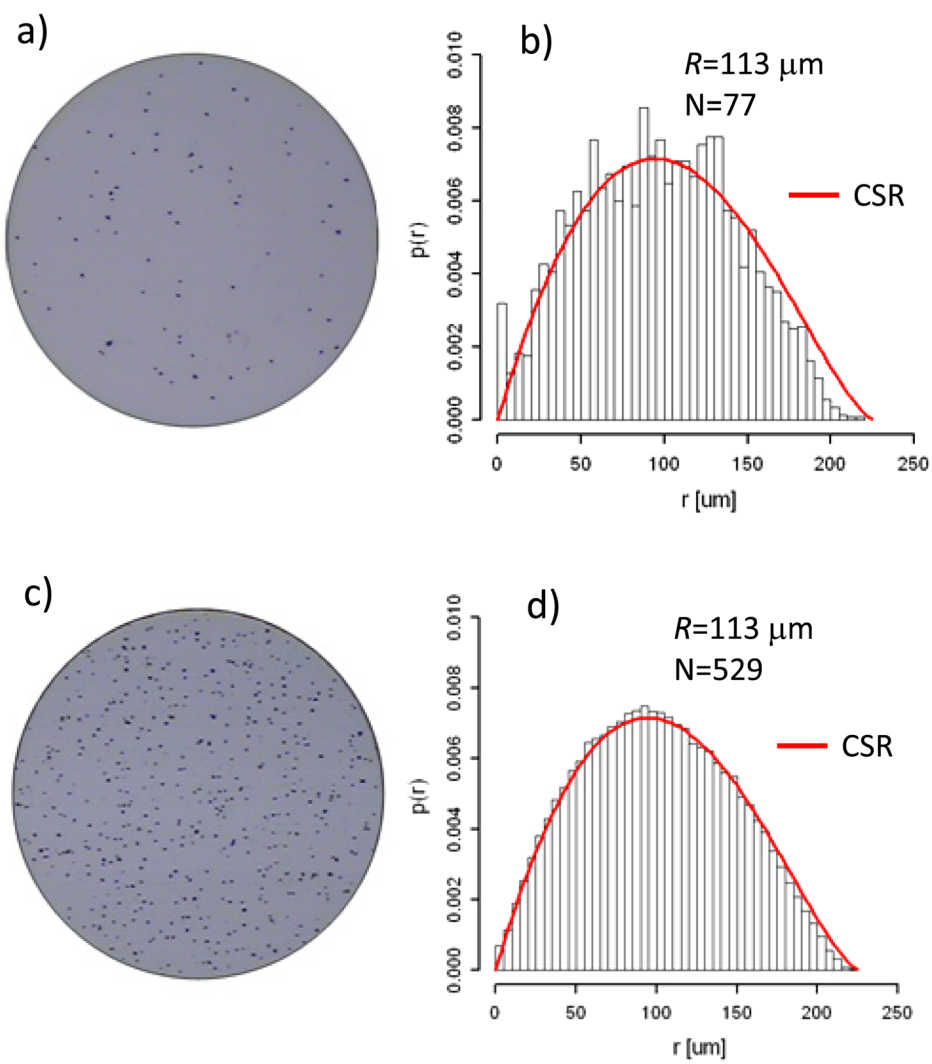

FIG. 1. (a) Breakdown spot distribution corresponding to a ramped voltage stressed device (0 V to 8 V) and (b) is the interevent distance histogram. The number of events is $N = 77$. (c) A similar device is stressed now from 0 V to 10 V. (d) is the corresponding interevent distance histogram. The number of events is $N = 529$. The solid curves were calculated using expression (1) with $R = 113\ \mu$m.

which corresponds to the probability density function (PDF) for the distances between randomly dropped points on a circle of radius R (see Appendix A). In Spatstat, the circular capacitor is represented by a single connected closed polygon with 128 vertices. Notice that the histograms do not agree completely with a CSR process, the most significant deviations occurring at the longest distances, and it is also clear that the difference reduces for a higher density of points. However, a central problem with this kind of approach, especially in the second case ($N = 529$), is that the large number of distances considered $N(N-1)/2 = 139656$ hinders the analysis of what is actually happening at the tails of the distribution.

In order to achieve a deeper insight into the point process characteristics, two conventional functional estimators are considered: first, F, the empty space function or point-event distance distribution and second, G, the nearest neighbor function or event-event distance distribution.[14] F is the cumulative distribution function (CDF) of the distance from a fixed point in the plane to the nearest point of the process and can also be interpreted as the probability that a randomly located disc of radius r contains at least one event. The estimate of F is a useful statistics summarizing the sizes of gaps in the pattern. On the other hand, G is the CDF of the distance from a typical point of the process to the nearest other point of the process. Deviations between the empirical and theoretical G curves may suggest spatial clustering or spatial regularity. F and G are estimators widely used in spatial statistics analysis. As it will be shown below, G can be generalized to higher neighbor orders. Remarkably, both F and G have the same CDF for a CSR process (see Appendix B),

$$F(r) = G(r) = 1 - \exp(-\lambda \pi r^2) \qquad r > 0, \tag{2}$$

where λ is the average point intensity. Notice that expression (2) assumes an unbounded observation window so that edge effects can in principle introduce some biasing in the estimators and in particular can lead to an overestimation of the mean nearest neighbor distance. This is similar to censoring effects in lifetime models.[8,15] A variety of edge-corrected estimators for F (Kaplan-Meier, Reduced Sample, Chiu-Stoyan) and G (Kaplan-Meier, Reduced Sample, Hanisch) have been proposed in the literature and they are illustrated in Fig. 2.[14] As it can be seen, the edge-corrected estimators do not differ significantly among them. Moreover, it will be shown below that edge-effects do not play a critical role in our case. However, notice that while the estimated F mainly deviates at the long distance range, G departs from CSR at the short distance scale. Remarkably, the estimated G for $N = 529$ (Fig. 2(d)) indicates that there are less nearest neighbors than expected for a Poisson process with the same average point intensity. This pseudo-inhibition of nearby points is in a large extent a consequence of having disregarded the size of the spots which can be in the range from 1 μm to 3 μm. As shown in Figs. 3(a) and 3(b), the metal electrode is completely molten at the failure sites and the modification of the metal electrode extends over a range of around 1.5 μm. As a consequence, the resulting structures are far more complicated than simple points. These micro-scale explosions, which in some cases exhibit a surrounding halo (see Fig. 3(b)), are consistent with early reports on the surface generation of BD spots in thick-oxide MOS devices[4] as well as with more recent gate oxide integrity studies.[5] Nevertheless,

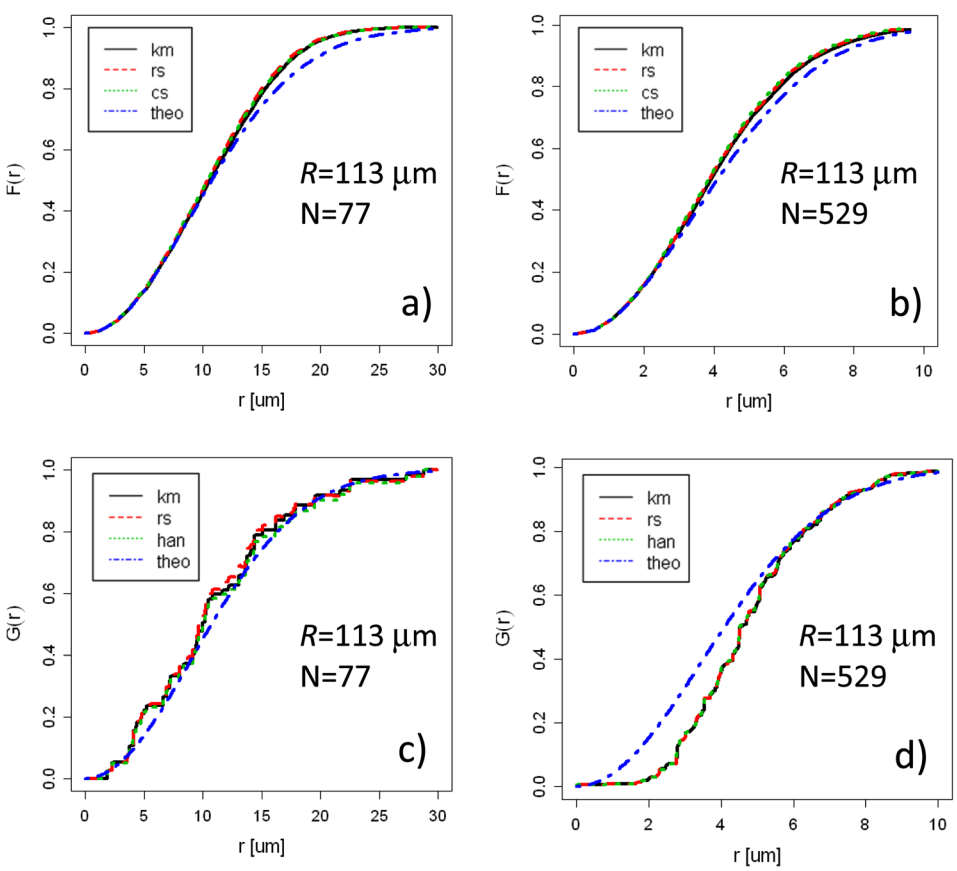

FIG. 2. (a) and (b) correspond to the point-event distance distribution F with $N = 77$ and $N = 529$ events, respectively. The point patterns are shown in Figs. 1(a) and 1(c). *km* refers to Kaplan-Meier, *rs* to Reduced Sample, *cs* to Chiu-Stoyan corrections, and *theo* to expression (2). (c) and (d) correspond to the event-event distance distribution G with $N = 77$ and $N = 529$ events, respectively. *han* refers to Hanish correction.

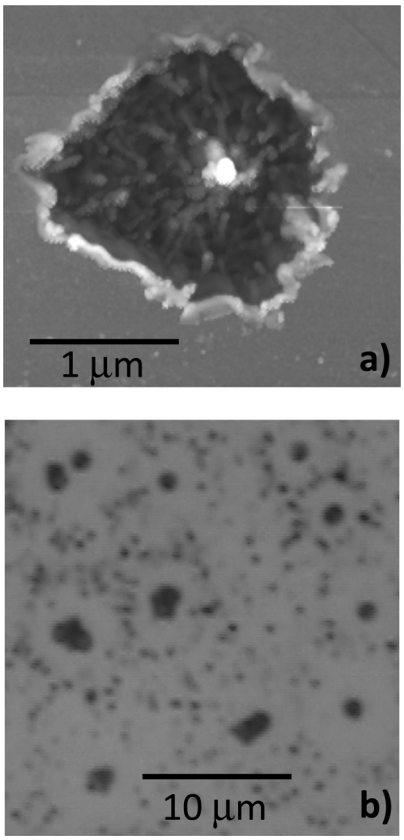

FIG. 3. (a) AFM image of a breakdown spot. (b) Distribution of BD spots as observed through an optical microscope.

a clear limitation of both the F and G estimators is the range of distances that can be analyzed, which for understandable reasons decreases as the number of point increases. In order to overcome this restriction, exploration of the distances to second nearest-neighbor, third nearest-neighbor, and even farther neighbors has been suggested as a way to investigate patterns at different scales.[16] As an illustrative example, Fig. 4 shows the kth-nearest neighbor distances for $k=1$ to $k=5$ for a typical BD spot pattern. Notice how the average distance between the joined points increases with the neighbor order. This multiscale approach will be used next to detect inhomogeneities in the spot pattern.

The CDF for the kth-nearest neighbor distance is given by the expression (see Appendix C),

$$G_k(r) = \frac{1}{(k-1)!}\Gamma(k, \pi\lambda r^2) \qquad k = 1, 2, 3...., \tag{3}$$

where Γ is the incomplete gamma function of order k. For $k=1$, the event-event distribution G given by expression (1) is recovered. To illustrate the effects of considering very dissimilar patterns on the G_k estimator, two cases are analyzed in detail. In this example, a device with radius $R = 282\ \mu$m has been stressed twice in order to increase the number of BD spots. Figures 5(a) and 5(b) show the corresponding intensity plot and the CDF G_k (k from 1 to 5) after the first stress ($N = 182$, $\lambda = 7.3\times10^{-4}$ points/μm^2), respectively. Notice that in this case, the nearest neighbor distances (solid lines) are shorter than expected for a CSR process with the same intensity (dashed lines), which is seemingly, although

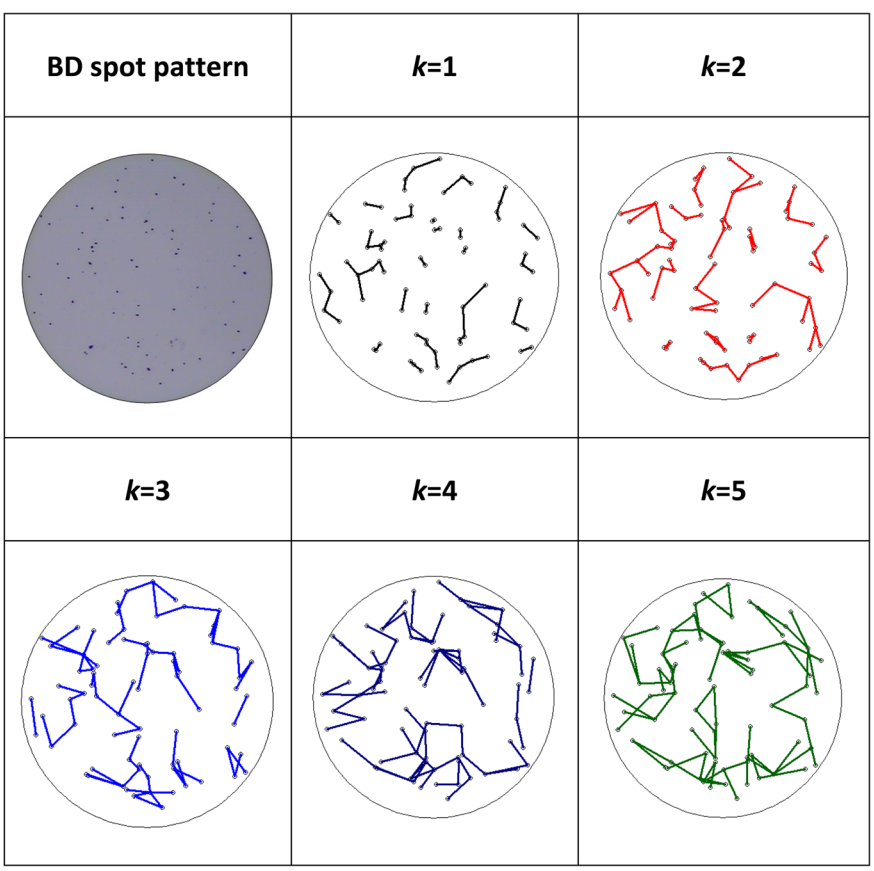

FIG. 4. Typical breakdown spot distribution and its kth nearest event map (k from 1 to 5).

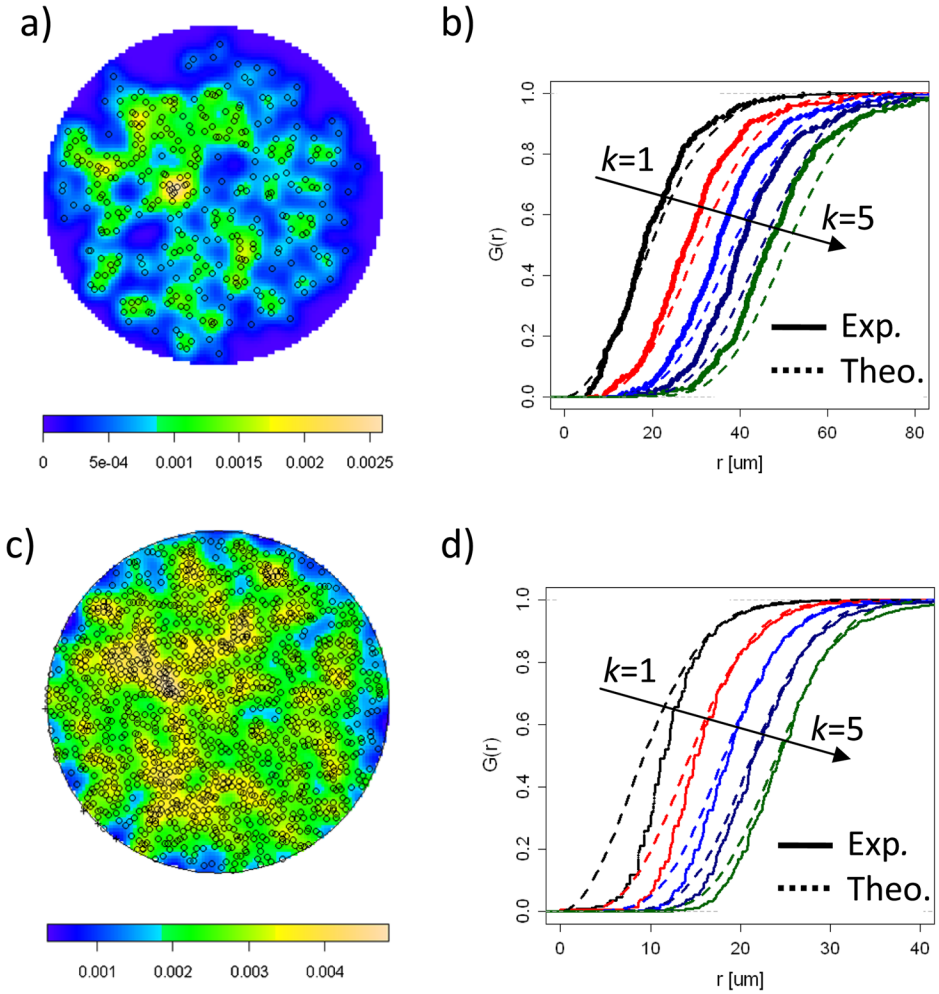

FIG. 5. (a) and (b) correspond to the intensity plot and the G_k (k from 1 to 5) distributions, respectively, for a device with $R = 282\,\mu$m and $N = 182$ events. (c) and (d) correspond to the same device after a second ramped voltage stress. In this case $N = 969$ events.

not conclusive, an indication of clustering. The difference between the empirical and theoretical curves increases for higher neighbor order. In fact, this is not a consequence of a genuine attraction process but a result of the low density of spots close to the periphery of the device. This observation is consistent with the larger than unity pair correlation function values reported in Ref. 9 for the same devices. In the case of Figs. 5(c) and 5(d), the point intensity is higher ($N = 969$, $\lambda = 3.9\times10^{-3}$ points/μm^2) and the empirical distances are longer than those for a CSR process. Again, this is because the size of the spots was neglected. As expected, this deviation reduces as the neighbor order increases and thus as the distance range under test increases. In order to show that the observed features do not arise because of a bounded observation window but as a consequence of the absence of points close to the periphery of the device and because of the finite size of the spots, Figs. 6(a) and 6(b) show G_k plots for two simulated point processes with $N = 200$. In the first case, the spots are generated just within an inner circle with a radius shorter ($0.9R$) than the actual device radius (see Fig. 6(a)). Notice that this particular distribution yields a parallel shift of the empirical G_k estimators toward the longer distance range. In the case of Fig. 6(b), the events are strictly mathematical points. No significant difference can be detected between the empirical and theoretical distributions for the typical device size and point number considered in this work.

Since a nonuniform BD spot distribution is apparently detected in our samples (see for example Fig. 5(c)), an immediate question arises concerning the significance of the average spot density calculated simply as the observed number of events over the area of the device: in what extent is this value a reliable measure of the process intensity given that the periphery of the devices exhibits such a peculiar behavior? In order to answer this question and to give a quantitative measure of this deviation, the following property of the estimator G_k is invoked:

$$r_k = \sqrt{\frac{k - \frac{1}{2}}{\lambda\pi}}, \tag{4}$$

where r_k is the distance corresponding to the mode (maximum of the PDF g_k) of the distribution for the kth-order event-event distribution (see Appendix C). Expression (4) can be rearranged as

$$A_k = \pi r_k^2 = \frac{1}{\lambda}\left(k - \frac{1}{2}\right), \tag{5}$$

where now, A_k is the area of the disc associated with the most frequent observed event-event distance at the order k. We call A_k the kth nearest neighbor disc area. Notice the linear relationship with slope $1/\lambda$ between A_k and k-0.5 expressed by Eq. (5). In this connection, Fig. 7 illustrates

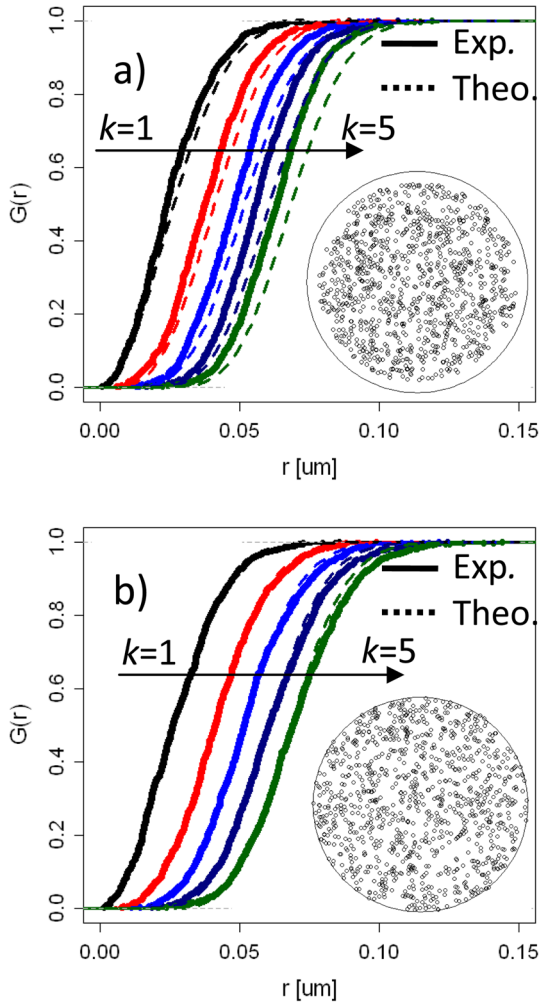

FIG. 6. Analysis of a simulated random point process with $N = 200$. (a) shows the G_k (k from 1 to 5) theoretical and empirical distributions for a process without points close to the periphery of the device. In (b), the points follow a spatial random process. Notice that no edge effect is observable.

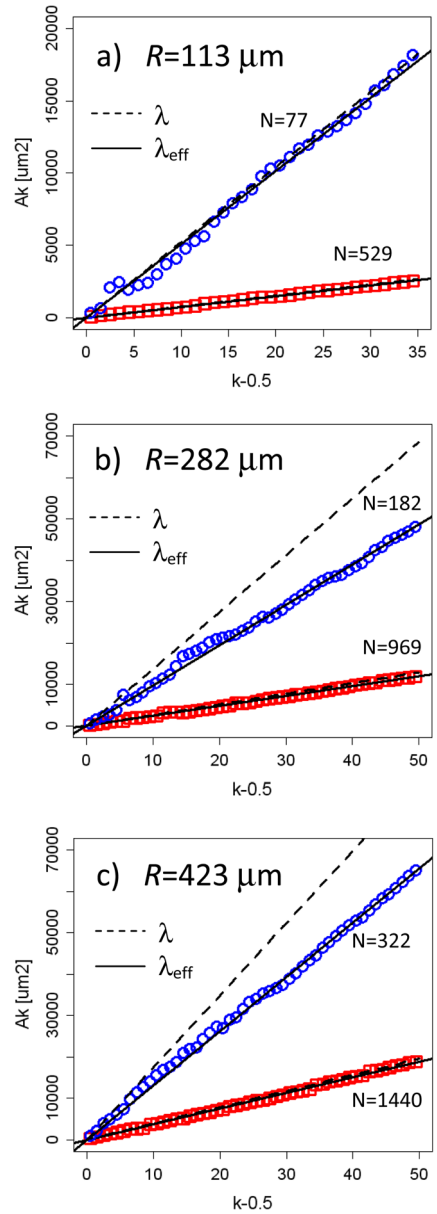

FIG. 7. Evaluation of the area of the disc corresponding to the kth nearest neighbor for devices with different radius and number of points: (a) $R = 113\ \mu$m with $N = 77$ and $N = 529$ points, (b) $R = 282\ \mu$m with $N = 182$ and $N = 969$ points, and (c) $R = 423\ \mu$m with $N = 322$ and $N = 1440$ events. The circles correspond to the lowest number of events while the squares to the highest number. The solid lines were obtained using expression (5) with λ_{eff} whereas the dashed lines were obtained with the same equation using $\lambda = N/A$, where N is the number of points and A the area of the device (see Table I for the parameter values).

three cases of interest (two of them revisited): (a) $R = 113\ \mu$m with $N = 77$ and $N = 529$ events, (b) $R = 282\ \mu$m with $N = 182$ and $N = 969$ events, and (c) $R = 423\ \mu$m with $N = 322$ and $N = 1440$ events. The circles correspond to the cases with the lowest density of spots, while the squares correspond to the highest density cases. The maximum order considered is $k = 50$ in order to avoid edge effects. The dashed lines are the theoretical values for A_k considering $\lambda = N/A$, where N is the number of events and A the area of the device. The solid lines in either case are linear fits to the experimental data from which the effective value λ_{eff} is calculated using Eq. (5). Table I summarizes the obtained results for the three samples with different damage levels investigated. Notice that $\lambda_{eff} > \lambda$ in all the cases. From λ_{eff}, and assuming for simplicity that the number of points remains unchanged, it is possible to estimate the effective radius R_{eff} of the most damaged device area. In Fig. 8, the experimental and theoretical lines corresponding to the highest density of spots are illustrated for comparison. In all the cases analyzed, $R_{eff} < R$ is obtained, which indicates a higher concentration of events towards the center of the structures. It is worth mentioning that the occurrence of a low-density BD spot region, which approximately consists in an outer annulus 10 μm width, can only be observed in the two largest area devices ($R = 282\ \mu$m and $R = 423\ \mu$m) analyzed. Even though there is no clear explanation yet on what causes this anomaly, it has been observed that severely stressed devices exhibit a huge accumulation of marks toward the center of the structure regardless of their shape, circular or rectangular. These results require further investigation but local dielectric constant deviations, thickness nonuniformities, or strain effects associated with the lift-off process could be behind the observed phenomenon. In principle, as reported in Ref. 9, the spatial scale of the fringing electric field at the

TABLE I. Summary of the obtained results. R is the nominal device radius, N the number of events detected, λ the average point intensity, λ_{eff} the effective average point intensity, and R_{eff} the effective radius of the damaged device area.

R [μm]	N	λ [μm^{-2}] = N/πR^2	λ_{eff} [μm^{-2}] from Eq. (5)	R_{eff} [μm] = $(N/\pi\lambda_{eff})^{0.5}$
113	77	1.92×10^{-3}	1.97×10^{-3}	111.52
	529	1.32×10^{-2}	1.35×10^{-2}	111.49
282	182	7.28×10^{-4}	1.02×10^{-3}	237.45
	969	3.88×10^{-3}	4.19×10^{-3}	271.10
423	322	5.73×10^{-4}	7.63×10^{-4}	366.54
	1440	2.56×10^{-3}	2.66×10^{-3}	414.63

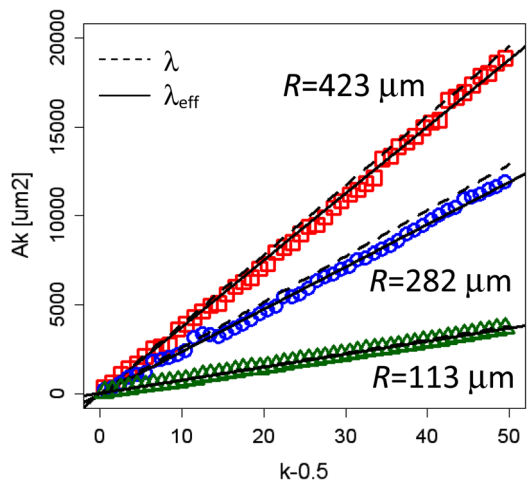

FIG. 8. Comparison of the area of the disc corresponding to the kth nearest neighbor for devices with different radius and the maximum number of points achieved. The solid lines were obtained using expression (5) with λ_{eff}, whereas the dashed lines were obtained with the same equation using $\lambda = N/A$ (see Table I for the parameter values).

edge of the capacitors does not seem to correlate to the spatial scale of the low BD spot density region.

IV. CONCLUSIONS

In this paper, it is has been shown that the assumption of a 2D homogeneous Poisson process for the breakdown spot spatial distribution in MIM structures does not always hold true. In order to demonstrate that deviations can indeed occur in such structures, a number of numerical and functional estimators like the event-event and point-event distributions were investigated. A novel methodology based on the analysis of the kth nearest neighbor disc area was shown to be useful to quantify the observed departures from complete spatial randomness. Finally, it is worth emphasizing that the method reported here is general and can be applied to any other system or structure exhibiting similar distribution of events.

ACKNOWLEDGMENTS

This work is funded in part by the Spanish Ministry of Science and Technology under contract number TEC2012-32305 and the DURSI of the Generalitat de Catalunya under contract number 2009SGR783. The authors also acknowledge I. M. Povey, E. O'Connor, and K. Cherkaoui from Tyndall National Institute, Cork, Ireland for their assistance during the oxide deposition and electrical characterization of the samples.

APPENDIX A: EVENT-EVENT DISTANCE DISTRIBUTION

The PDF of the distance r between two points randomly dropped on a circle of radius R is derived here using Crofton's theorem.[17] If P is the probability that the two points are separated by a distance between r and $r + \Delta r$ and P_1 is the same probability when one of the points is on the circumference of the circle then,

$$AdP = 2(P_1 - P)dA, \tag{A1}$$

where $A = \pi R^2$ is the area of the circle and $dA = 2\pi R dR$ the differential area. Since the area of the annulus section$S$in Fig. 9 is

$$S = 2\arccos\Big(r/(2R)\Big)r\Delta r \tag{A2}$$

the probability P_1 is given by

$$P_1 = \frac{S}{\pi R^2} = \frac{2r\Delta r\cos^{-1}(r/(2R))}{\pi R^2}. \tag{A3}$$

Substituting expression (A3) into Crofton's formula (A1) and rearranging terms we get

$$R^4 dP + 4R^3 P dR = \frac{8r\Delta r R\cos^{-1}(r/(2R))}{\pi}, \tag{A4}$$

which after integrating and using the zero-probability event $p = 0$ for $r = 2R$ yields

$$p(r) = \frac{2r}{R^2}\left[\frac{2}{\pi}\cos^{-1}\left(\frac{r}{2R}\right) - \frac{r}{\pi R}\sqrt{1 - \frac{r^2}{4R^2}}\right] \qquad 0 < r < 2R. \tag{A5}$$

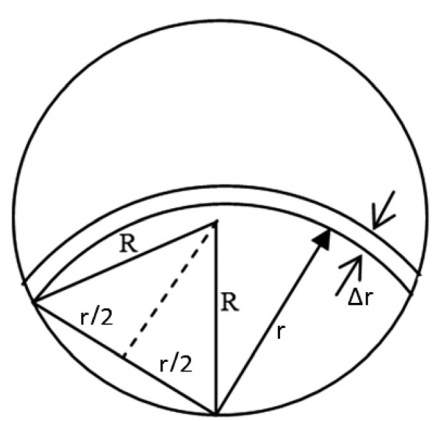

FIG. 9. Scheme for the calculation of the interevent distance distribution of randomly dropped points on a circle of radius R.

Integrating Eq. (A5), we can also calculate the CDF $P(r)$

$$P(r) = 1 + \frac{2}{\pi}\left(\frac{r^2}{R^2} - 1\right)\cos^{-1}\left(\frac{r}{2R}\right) - \frac{r}{\pi R}\left(1 + \frac{r^2}{2R^2}\right)\sqrt{1 - \frac{r^2}{4R^2}} \qquad 0 < r < 2R. \quad \text{(A6)}$$

APPENDIX B: CONTACT DISTRIBUTION

Let $P(r)$ be the probability of finding no points within a distance $r$of some fixed point (see Fig. 10). For a CSR process with intensityλ, the probability that there will be a point in an infinitesimal annulus between the distances r and $r + \Delta r$ is $2\pi\lambda r\Delta r$. The probability that there are no points within $r + \Delta r$ is by independence the probability that there are no points within $r$times the probability that no point occurs in the region between r and $r + \Delta r$, that is,

$$P(r + \Delta r) = P(r)(1 - 2\pi\lambda r\Delta r). \quad \text{(B1)}$$

Considering $\Delta r \to 0$, we arrive at the differential equation

$$\frac{dP(r)}{dr} = -2\pi\lambda r P(r), \quad \text{(B2)}$$

which, under the condition $P(r = 0) = 1$, gives

$$P(r) = \exp(-\pi\lambda r^2). \quad \text{(B3)}$$

The empty space function or point-event distribution is defined as $F(r) = 1 - P(r)$, that is,

$$F(r) = 1 - \exp(-\pi\lambda r^2). \quad \text{(B4)}$$

Therefore, the PDF for the contact distribution is given by the expression

$$f(r) = 2\pi\lambda r\exp(-\pi\lambda r^2). \quad \text{(B5)}$$

APPENDIX C: *k*th NEAREST NEIGHBOUR DISTRIBUTION

For a CSR process with intensity λ, the probability of having at least k points in a circle of area $A = \pi R^2$ is given by

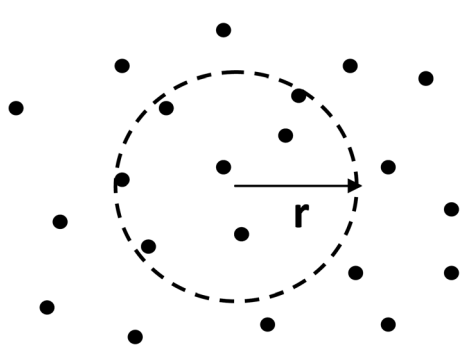

FIG. 10. Scheme for the calculation of the point-event distance distribution F. r is the distance from an arbitrary point of the plane (which does not necessarily coincide with a point of the process) to another arbitrary point of the plane.

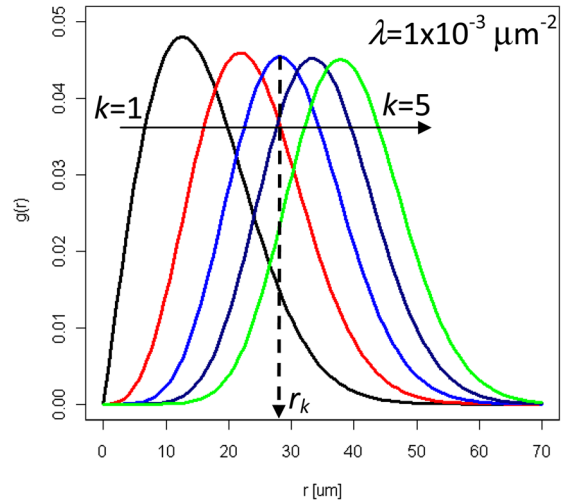

FIG. 11. Plot of the theoretical PDF distribution g (Eq. (C3)) for the nearest neighbor event (k from 1 to 5). r_k is the maximum of the distribution.

$$P(n, A) = 1 - \sum_{i=0}^{k-1}\frac{(\lambda A)^i}{i!}\exp(-\lambda A). \quad \text{(C1)}$$

The probability that the kth nearest point is found in the interval $r + \Delta r$ equals to the probability that this point is located in the annulus with inner and outer radius r and $r + \Delta r$, respectively. Assuming $\Delta r \to 0$, we get

$$P(k, k \in \Delta A) = P(k, \pi(r + \Delta r)^2) - P(k, \pi r^2), \quad \text{(C2)}$$

which after differentiating with respect to r yields

$$g_k(r) = \frac{2(\pi\lambda)^k}{(k-1)!}r^{2k-1}\exp(-\pi\lambda r^2) \qquad k = 1, 2, 3..... \quad \text{(C3)}$$

Equation (C3) gives the PDF of the distance from an arbitrarily chosen point to its kth nearest neighbor (see Fig. 11). r_k is the maximum of g_k and is given by expression (4). Remarkably, substituting $m = \pi\lambda r^2$ in Eq. (C3) yields

$$g_k(r) = \frac{m^{k-1}}{(k-1)!}\exp(-m) \qquad k = 1, 2, 3...., \quad \text{(C4)}$$

which corresponds to the Erlang distribution of order k. Finally, the CDF reads

$$G_k(r) = \frac{1}{(k-1)!}\Gamma(k, \pi\lambda r^2) \qquad k = 1, 2, 3...., \quad \text{(C5)}$$

where $\Gamma(k, t) = \int_0^x t^{k-1}e^{-t}dt$ is the lower incomplete gamma function of order k. For $k = 1$, we obtain the event-event CDF

$$G(r) = 1 - \exp(-\lambda\pi r^2). \quad \text{(C6)}$$

[1]A. Oates, "Reliability issues for high-K gate dielectrics" in *IEEE International Electron Devices Meeting, 2003. IEDM '03 Technical Digest* (IEEE, 2003), pp. 38.2.1–38.2.4.
[2]E. Miranda and J. Suñé, "Electron transport through broken down ultra-thin SiO_2 layers in MOS devices," Microelectron. Reliab. **44**, 1–23 (2004).

[3]S. Lombardo, J. Stathis, B. Linder, K. Leon Pey, F. Palumbo, and C. H. Tung,. "Dielectric breakdown mechanisms in gate oxides," J. Appl. Phys. **98**, 121301 (2005).
[4]N. Klein and H. Gafni, "The maximum dielectric strength of thin silicon oxide films," IEEE Trans. Electron. Devices **13**, 281–289 (1966).
[5]S. Huth, O. Breitsenstein, A. Huber, and U. Lambert, "Localization of gate oxide integrity defects in silicon metal-oxide-semiconductor structures with lock-in IR thermography," J. Appl. Phys. **88**, 4000–4003 (2000).
[6]X. Zhu, W. Su, Y. Liu, B. Hu, L. Pan, W. Lu, J. Zhang, and R. Li, "Observation of conductance quantization in oxide-based resistive switching memory," Adv. Mater. **24**, 3941 (2012).
[7]K. Kim, D. Jeong, and C. Hwang, "Nanofilamentary resistive switching in binary oxide system: a review on the present status and outlook," Nanotechnology **22**, 254002 (2011).
[8]P. Diggle, *in Statistical Analysis of Spatial Point Patterns* (Arnold, 2003).
[9]E. Wu, J. Stathis, and L. Han, "Ultra-thin oxide reliability for ULSI applications," Semicond. Sci. Technol. **15**, 425 (2000).
[10]J. Suñé and E. Wu, "Statistics of successive breakdown events in gate oxides," IEEE Electron. Devices Lett. **24**, 272 (2003).
[11]M. Alam, D. Varghese, and B. Kaczer, "Theory of breakdown position determination by voltage- and current-ratio methods," IEEE Trans. Electron. Devices **55**, 3150 (2008).
[12]E. Miranda, E. O'Connor, and P. K. Hurley, "Analysis of the breakdown spots spatial distribution in large area MOS structures," in IEEE International Reliability Physics Symposium (IRPS) (IEEE, 2010), pp. 775–777.
[13]E. Miranda, D. Jiménez, J. Suñé, E. O'Connor, S. Monaghan, I. Povey, K. Cherkaoui and P. K. Hurley, "Nonhomogeneous spatial distribution of filamentary leakage paths in circular area Pt/HfO_2/Pt capacitors," J. Vac. Sci. Technol. B **31**, 01A107 (2013).
[14]J. Illian, A. Penttinen, H. Soyan, and D. Stoyan, *in Statistical Analysis and Modelling of Spatial Point Patterns* (Wiley, 2008).
[15]A. Baddeley and R. Turner, "Spatstat: an R package for analyzing spatial point patterns," J. Stat. Software **12**, 1 (2005). Available at http://www.jstatsoft.org/v12/i06/.
[16]P. Dixon, "Nearest neighbor methods," in *Encyclopedia of Environmetrics* (John Wiley & Sons, 2013), doi: 10.1002/9780470057339.van007.pub2.
[17]H. Solomon, in *Geometric probability*, CBMS-NSF Regional Conference Series in Applied Mathematics Vol. 28 (Siam, 1978).